Butterfly wing iridescence is regulated by *araucan*, a direct target of Optix and Spalt

Martik Chatterjee[1,4], Cédric Finet[2], Kate J. Siegel[1], Ling Sheng Loh[3], Seydeanna Delgado[1], Jeanne M.C. McDonald[1], Eirene Markenscoff-Papadimitriou[4], Antónia Monteiro[2], and Robert D. Reed[1]

[1]Department of Ecology and Evolutionary Biology, Cornell University, Ithaca, NY,14853, USA;

[2]Department of Biological Sciences, Faculty of Science, National University of Singapore, Singapore, 117543, Singapore

[3]Department of Biological Sciences, Colombian College of Arts and Sciences, George Washington University, Washington, D.C, 20052, USA

[4]Department of Molecular Biology and Genetics, Cornell University, Ithaca, NY, 14853, USA

Correspondence

Robert D. Reed, Department of Ecology and Evolutionary Biology, Cornell University, 215 Tower Road, Ithaca, NY, 14853
Email: robertreed@cornell.edu

Martik Chatterjee, Department of Ecology and Evolutionary Biology, Cornell University, 215 Tower Road, Ithaca, NY, 14853
Email: mc2548@cornell.edu

Keywords

structural coloration, butterfly wing patterns, Iroquois-complex, evo-devo

ABSTRACT

Butterfly wings exhibit a remarkable diversity of structural iridescent colors, yet the genetic regulation of iridescence remains poorly understood. Here, we show that the Iroquois-complex transcription factor Araucan plays a specific and essential role in modulating wing scale iridescence in the common buckeye butterfly, *Junonia coenia*. Using CRISPR-Cas9 knockouts, we demonstrate that loss of *araucan* function causes dorsal wing scales to shift from golden-brown to blue iridescence, and eyespot center scales to shift from saturated purple-violet to dull grey-brown. These phenotypes are associated with thickness of the lower lamina in scale cells, a structural feature known to influence thin-film interference, along with reduction of pigmentation in ground scales. We further show that the patterning transcription factors Optix and Spalt bind to the *araucan* promoter during wing development, suggesting they may regulate *araucan* expression in a color pattern-specific manner. Together, our findings identify *araucan* as a critical effector of scale ultrastructure, structural coloration, and pigmentation in butterflies and provide new insights into how core wing patterning genes may control the evolution of iridescence.

ARTICLE SUMMARY

This study investigates how butterflies produce iridescent colors on their wings. The authors used gene editing to disrupt the function of *araucan*, a transcription factor, in the butterfly *Junonia coenia*. They found that *araucan* controls wing scale structure and is essential for producing specific hues of iridescence. Loss of *araucan* changed brown scales to blue and purple eyespot scales to grey by changing the thickness in the lower layer of the scale. The authors also show that two known wing patterning transcription factors, Optix and Spalt, bind to the *araucan* promoter, suggesting a regulatory pathway for the control of structural color.

INTRODUCTION

Coloration in animals serves as a powerful model for understanding how gene regulatory networks give rise to complex, adaptive traits. Colors are most commonly generated by pigmentation, by structural features that manipulate light, or through a combination of both. Although structural coloration is widespread across the animal kingdom—particularly in insects—its genetic and developmental bases remain poorly understood (Finet 2024). Butterfly wings, with their nanostructured scales and vivid structural organization that produce blue, purple, and green hues, offer an ideal system for uncovering how genes shape the physical traits that underlie these colors.

Over the past decade, advances in genomic mapping and CRISPR-Cas9 gene editing have enabled the discovery and functional validation of key genes and regulatory elements involved in butterfly wing pigmentation and pattern variation. Comparative studies and insights from model insects such as *Drosophila melanogaster* have further expanded the developmental genetic framework for wing patterning. However, the genetic basis of structural coloration remains less well resolved, with only a handful of causative genes identified across a few butterfly species. These include *optix*, a regulator of blue iridescence in *Junonia coenia* (Zhang et al. 2017; Thayer et al. 2020) and silver scale development in *Speyeria mormonia* (Livraghi et al. 2025); *bric-a-brac* and *doublesex* in the control of UV-reflecting scales in *Colias spp.* (Ficarrotta et al. 2022) and *Zerene spp.* (Rodriguez-Caro et al. 2021), respectively ; and *antennapedia*, *apterousA*, *doublesex*, *ultrabithorax*, *optix*, and *hr38* in regulating silver reflectance in *Bicyclus anynana* (Prakash et al. 2022; Prakash et al. 2024).

Here, we investigate the role of *araucan/caupolican* (also known as *iroquois2*), a gene encoding the homeodomain transcription factor of the *Iroquois* family, in the wing color patterning of the common buckeye butterfly *J. coenia*. Most hexapods, including butterflies, possess two *Iroquois* genes—one orthologous to *D. melanogaster's mirror* (*iroquois1*) and one to *araucan/caupolican* (*iroquois2*). In *D. melanogaster*, however,

iroquois2 has undergone a lineage-specific duplication, giving rise to the paralogs *araucan* and *caupolican* (Kerner et al. 2009; Setton et al. 2024; Chatterjee et al. 2025). The three *Iroquois* genes (*araucan*, *caupolican*, and *mirror*) in *Drosophila* regulate multiple developmental processes, including dorsal notum patterning, longitudinal wing vein specification, and posterior wing domain (alula) identity (Gómez-Skarmeta et al. 1996; Gómez-Skarmeta and Modolell 1996; Kehl et al. 1998; Cavodeassi et al. 2001; Ikmi et al. 2008). Recent findings suggest that *mirror* specifies a far posterior domain in butterfly wings—a role likely ancestral in broad winged insects but lost in *D. melanogaster* and other calyptrate flies due to evolutionary reductions in wing complexity (Chatterjee et al. 2025). Despite its consistent expression in the basal part of the wing across wing development in *Heliconius* butterflies (Hines et al. 2012), the function of *araucan/caupolican* (hereafter *araucan*) in butterflies remains unknown.

In this study, we used CRISPR-Cas9 mutagenesis and gene expression analyses to investigate the role of *araucan* in wing coloration in *J. coenia*. We show that *araucan* is a necessary regulator of wing scale ultrastructure, specifically influencing the thickness of the lower lamina—a critical determinant of iridescent hue. Our findings identify *araucan* as a novel regulator of structural coloration in butterflies and provide the first functional evidence for this gene outside of *Drosophila*, highlighting its evolutionary flexibility and specialized role in modulating scale-based structural color traits.

MATERIALS AND METHODS

Identification of *Iroquois* complex genes

We previously identified the *Iroquois* complex genes in *J. coenia* (Chatterjee et al. 2025). For this study, we used an updated annotation (Fandino et al. 2024), which resulted in revised gene model identifiers for the *Iroquois* complex. We identified the *J. coenia* gene *JC_g12213* as the single ortholog of *D. melanogaster araucan/caupolican* paralogs (Fig. S1). For clarity and consistency, we refer to *JC_g12213* as *araucan* in *J. coenia*, with the understanding that it is equally related to both the paralogs in *D. melanogaster*. The updated phylogeny and sequence information used for orthology

assignments are provided in Fig. S1 and File S1, respectively. To ensure reproducibility and compatibility with future genome releases, we have provided both the predicted amino acid and coding DNA sequences of *araucan* in the supplementary materials (File S1).

CRISPR-Cas9 mutagenesis of *J. coenia araucan*

To assess the function of *araucan* in *J. coenia* we generated CRISPR-Cas9 somatic mosaic deletions targeting the *araucan* coding region. We used a previous protocol where early embryos are injected with single guide RNAs (sgRNAs) and Cas9 enzyme (Zhang and Reed 2017). Mutations induced in early syncytial embryos typically only affect a subset of nuclei, resulting in mosaic knockout (mKO) animals.

We designed two sgRNAs – 5'-CTGGGTACGATTTAGCAGCC-3' and 5'-CTCCTGCTCCTTGTCCTCGT-3' – to target the exon of *araucan* containing the conserved homeobox domain in *J. coenia* (Fig. S1a). Possible off target sgRNAs were ruled out by blasting against the *J. coenia* genome assembly. sgRNAs were synthesized by Integrated DNA Technologies, Inc. (Coralville, IA, USA), rehydrated in 1x Tris-EDTA buffer, and mixed with Alt-R S.p. Cas9 Nuclease/Nickase (Integrated DNA Technologies, Inc., Coralville, IA, USA) to a final concentration of 200ng/ul sgRNA and 500ng/ul Cas9.

We collected eggs by placing leaves of *Plantago lanceolata* in a cage with gravid females for 1-2 hours, and then prepared eggs for microinjection by submersing them in 5% benzalkonium chloride (Sigma-Aldrich, St Louis, MO, USA) for 30s followed by a wash with distilled water. Prepared eggs were then lined up on double sided tape on glass slides and sgRNA and Cas9 mixture was injected into the eggs using 0.5-mm borosilicate needle (Sutter Instruments, Novato, CA, USA) and a PLI-100 Picoinjector (Harvard Apparatus, Holliston, MA, USA). Injections were completed within 2-3hrs after oviposition, and larvae from injected eggs were raised on artificial diet at 27°C, 70% humidity, and a 16hr : 8hr light : dark cycle. Adults were frozen upon emergence, and

phenotyped and imaged using a Keyence VHX-7000 microscope.

Genotyping CRISPR mutants

We genotyped *J. coenia* mosaic knockout (mKO) mutants to confirm Cas9-induced deletions in the *araucan* gene. Mutants “mKO A” and “mKO 3” were selected based on their blue cover scale phenotypes (Fig. S2), while “mKO M” was chosen for its symmetrically disrupted eyespot phenotype (Fig. S3). We extracted DNA (OMEGA BIO-TEK, Norcross, GA, USA) from the thoracic flight muscles of butterflies that showed obvious wing pattern anomalies compared to wild types. We used PCR to amplify DNA from around the potential cut sites using the primers 5’-ATACTAAACCCTGCACCCGC-3’ and 5’-ACGTACTCACAAGCGAACGT-3’. We ran amplified DNA from wild type and mutant individuals on an agarose gel and purified (Monarch DNA Extraction and Purification kit, new England Biolabs, MA, USA) and cloned the PCR products into JM109 competent cells using pGEM®-T Easy Vector Systems (Promega Corporation, Madison, WI, USA). Transformed cells were amplified and Sanger sequenced at the Genomics Facility, Cornell Institute of Biotechnology, Ithaca, NY, USA.

Micro-spectrophotometry of wild type and *araucan* mutant scales

We mounted individual wing scales from wild-type and *araucan* mutant *J. coenia* butterflies on glass slides and measured their normal-incidence reflectance spectra using a mercury-xenon light source (Thorlabs, New Jersey, USA) connected to a uSight-2000-Ni micro-spectrophotometer (Technospex Pte. Ltd., Singapore). We used a Nikon TU Plan Fluor 100× objective (numerical aperture = 0.9) to collect spectra and calibrated the setup with a dielectric mirror. For each measurement, we averaged 10 scans with an integration time of 100 ms. We recorded three measurements from different locations on each of three scales per genotype and averaged them to obtain a representative reflectance spectrum.

To measure absorbance, we used the same optical setup with a 20× objective (NA = 0.5). We mounted individual scales submerged in clove oil (Hayashi Pure Chemical Ind., Ltd.) between a slide and coverslip to match the refractive index of chitin and used

a clove oil-covered transparent area of the slide as a reference. For each genotype, we measured three locations on each of five scales and averaged the data to generate absorbance spectra.

We performed all spectral analysis and visualization using the pavo 2 package in R (Maia et al. 2019). To test for significant differences in spectral values between wild-type and *araucan* mutant scales, we conducted independent two-sample t-tests at each 50 nm increment from 350 to 700 nm. We applied the Benjamini-Hochberg False Discovery Rate (FDR) method to adjust p-values for multiple comparisons and considered adjusted p-values < 0.05 as significant.

Transverse sectioning and scanning electron microscope imaging of *araucan* mutant and wild type scales

We used scanning electron microscopy (SEM) to assess structural differences between wild-type and *araucan* mutant scales. We mounted individual scales from mutant mosaic clones and contrasting wild-type regions on carbon tape and sputter-coated them with platinum (JEOL JFC-1600) for 30 s at 30 mA. We imaged the samples using a FEI Versa 3D with the following parameters: voltage 10 kV, current 32 pA. To obtain transverse-sections of wing scales, we used Focused Ion Beam (FIB) milling with the gallium ion beam of the FEI Versa 3D, applying a beam voltage of 8 kV, beam current of 25 pA, and a tilt of 52°. We performed the FIB-SEM in the Electron Microscopy Facility, National University of Singapore.

We obtained the transverse section of the scales shown in Fig. 1c by cryo-fracturing the scales following a previously described protocol (Ren et al. 2020). We then mounted whole and cryo-fractured scales of interest on carbon tape and sputter-coated them with an 8 nm layer of gold using a Cressington 208HR Sputter Coater. We acquired images on an FEI Teneo LV SEM using the Everhard Thornley detector and beam parameters of 5.00 kV/6.3 pA with a 10 µs dwell time. We used cryo-fracturing only to generate the image used in Fig. 1c. All measurements for laminar thickness reported were done on scales that were milled using FIB and imaged using SEM.

Measurement of scale ultrastructure and statistical analysis

We quantified scale ultrastructure by measuring three parameters: lower lamina thickness (LL), inter-ridge distance (d_{RR}), and crossrib ($d_{CR\text{-}CR}$) spacing (Fig. 1c; Fig. 1d). We performed all measurements in Fiji using the line tool (Schindelin et al. 2012). Lower lamina thickness was corrected for tilted perspective (measured thickness/sin 52°) (Villinger et al. 2012). For each genotype (wild type and *araucan* mutant), we analyzed five individual scales per wing region and scale type. From each scale, we recorded 10 measurements of lower lamina thickness, 25 measurements of inter-ridge distance, and 50 measurements of crossrib spacing. We collected measurements from cover and ground scales in the forewing eyespot center, and from cover scales in the dorsal non-eyespot region.

We analyzed scale ultrastructure data using linear mixed-effects (LME) models implemented in the R package nlme (Pinheiro et al. 1999; version) et al. 2025) which accounts for hierarchical data structures. For each geometric parameter (lower lamina thickness, inter-ridge distance, and crossrib spacing), we treated scale type as a fixed effect and included scale identity nested within individual butterfly as a random effect. To address heteroscedasticity among scale types, we applied the varIdent() function. We selected the best-fitting model based on the Akaike Information Criterion (AIC). We conducted pairwise comparisons of group means using the multcomp R package. We report p-values and 95% confidence intervals for all pairwise comparisons in Tables 1 and 2. A summary of the fixed effects from the linear mixed-effects models, including degrees of freedom, F-values, and p-values, is provided in Supplementary Tables S2 and S3. Raw measurement data are also included to support independent reanalysis (see Data Availability).

Hybridization chain reaction fluorescent *in situ* hybridization of *araucan*

We designed a hybridization chain reaction (HCR) probe set targeting the coding sequence of *J. coenia araucan* using 30 pairs of 25 bp probes (50 bp per site) spanning the annotated transcript (File S2). We ordered the probes as pooled oligonucleotides

from IDT. We confirmed probe specificity using BLAST against the most recent *J. coenia* genome assembly, ensuring no off-target binding sites.

For HCR experiments, we dissected last instar larval imaginal discs, as well as pupal wings at 13% (first day post-pupation) and 25% (second day post-pupation) of pupal development. We used *araucan* probes paired with B1 initiators and visualized them with Alexa Fluor 647-labeled hairpins. As a positive control, we used *spalt* probes labelled with B3 initiators (File S2) and visualized them in the 546 nm channel. We performed co-detection of *araucan* and spalt expression in wings from one side of each individual, while using the contralateral wings as negative controls. In these controls, we omitted the probes but followed all other HCR steps to assess background fluorescence. We performed the HCR following the protocol described by Bruce et al (dx.doi.org/10.17504/protocols.io.bunznvf6). We acquired high magnification images for Fig. 3 using a Leica Stellaris 5 confocal microscope in the laboratory of Dr. Eirene Markenscoff-Papadimitriou (Department of Molecular Biology and Genetics, Cornell University). To capture for pattern specific expressions across the entire wing tissue in Fig. S4 we used a Keyence BZ-X800 fluorescence microscope in the laboratory of Dr. Anyi Mazo-Vargas (Department of Biological Sciences, Duke University).

Chromatin immunoprecipitation and sequencing

We collected 40-44 last instar larval wings discs per replicate and 8-10 day-5 old pupal wings (65 % pupal development) per replicate and fixed them in formaldehyde and quenched with glycine for chromatin immunoprecipitation sequencing (ChIP-seq), as previously described (Lewis et al. 2016). Following the protocol of Lewis et al. (Lewis et al. 2019), we then homogenized the fixed tissues using a dounce homogenizer and lysed them in lysis buffer. To shear the chromatin, we sonicated the lysates using a Bioruptor sonicator (Diagenode) at the highest setting for 5 minutes, with 30-second on/off cycles. Based on our previous optimization for butterfly wing tissue, these settings consistently produce DNA fragments between 200-700 bp, suitable for ChIP-seq. We incubated 15–20 µg of sheared DNA from larval wing discs overnight with a rabbit anti-Spalt antibody (generously provided by Dr. Michael Perry, University of California, San

Diego, USA). We incubated a similar amount of sheared DNA from pupal wings with a rat anti-Optix antibody (Martin et al. 2014). As a positive control for both developmental stages, we also incubated sheared DNA with a mouse anti-RNA polymerase II antibody (ab5408; Abcam, Boston, MA, USA). To assess background binding, we prepared our Input negative controls by incubating 2-5 µg of sheared DNA with Dynabeads™ Protein A and Protein G (ThermoFisher Scientific Inc.). Following overnight antibody incubation, we performed immunoprecipitation using Dynabeads™ Protein A and Protein G at a 1:1 ration We then washed the immunoprecipitated DNA with a series of salt buffers, treated it with Proteinase K, and carried out reverse crosslinking at 65 °C overnight. We extracted DNA from all ChIP, input, and control samples using a column-based purification kit (#14209; Cell Signaling Technology, Inc.). We prepared sequencing libraries from the purified DNA using the NEBNext Ultra II DNA Library Prep Kit (New England Biolabs), following the manufacturer's protocol without size selection, and amplified libraries using 13 PCR cycles. Quality control of the prepared libraries were performed using an Agilent Fragment Analyzer to check for size distribution and subsequently sequenced by Biotechnology Resource Center (BRC) Genomics Facility (RRID:SCR_021727) at the Cornell Institute of Biotechnology, Cornell University on their Illumina NextSeq 500 platform using a read length of 2 x 32 bp, resulting in a read depth of more than 30 million read pairs (60 million total reads) per sample.

ChIP-seq data processing, visualization and peak calling

We aligned raw sequencing reads to the *J. coenia* Version 2 genome assembly (available on Lepbase.org; refer to Data Availability) using Bowtie 2 (Langmead and Salzberg 2012). We filtered for uniquely mapping read pairs using a custom Python script previously described (Lewis and Reed 2019), and removed PCR duplicates using the “MarkDuplicates” function in Picard Tools. For each replicate, we called peaks enriched over background input using MACS3 (Zhang et al. 2008) with a relaxed false discovery rate (FDR) threshold of q = 0.05. To identify high-confidence peaks consistently enriched across replicates, we applied Irreproducible Discovery Rate (IDR) analysis to the MACS3 output (Li et al. 2011). To visualize genome-wide transcription factor binding, we generated ChIP signal tracks using the “bamCompare” function in

deepTools (Ramírez et al. 2016). We calculated either the difference between ChIP and Input signals (--operation subtract) or their $\log_2$ enrichment (--operation log2), after normalizing read coverage using RPKM (--normalizeUsing RPKM). We visualized the resulting bigWig files in Integrative Genomics Viewer (Robinson et al. 2011), overlaying them with IDR-filtered peaks to highlight regions of significant binding and read pileup at shared genomic loci.

RESULTS

araucan knockouts result in iridescent blue scales via laminar thickening

We injected 596 eggs with Cas9 and *araucan* sgRNAs, of which 141 hatched and 92 survived to adulthood. Fourteen of the adults that emerged had wing color mutations. We observed two distinct classes of mutations, both of which involved iridescent coloration: (1) blue iridescence in mutant clones across the dorsal wing surface, and (2) a shift from purple-violet to grey-brown specifically in eyespot centers. Genotyping confirmed that individuals from both mutant classes had lesions at the sgRNA sites in the *araucan* coding region (Fig. S1c).

Out of the fourteen mKO butterflies we observed, nine individuals showed mosaic clones of blue iridescence, exclusively on dorsal hind wing surfaces (Fig. 1a, S2). Since iridescent blue colored scales can be artificially selected for in populations of *J. coenia* (Thayer et al., 2020), we assessed individuals from our wild type colony for similar iridescent scales. Out of the individuals randomly observed (n = 32), we did not observe any blue iridescent scales on the dorsal surface of the hind wings, which supports that the blue iridescence in the mKOs is a result of knockdown of *araucan* (chi-squared test, $p < 0.005$). This conclusion was also supported by the fact that individuals with iridescent patches of scales presented this phenotype asymmetrically (Fig. S2), consistent with cell linages mosaicism (Zhang, Mazo-Vargas, et al., 2017), whereas natural variation in iridescence is typically symmetrical.

The shift from golden-brown scales in the wild type to vivid blue in the mutant was

quantified using reflectance spectrophotometry. Mutant scales exhibited increased reflectance in the ultraviolet and blue wavelengths (< 500 nm), while wild-type scales reflected more light in longer wavelengths (> 500 nm), consistent with their golden-brown appearance (Fig. 1b). To determine whether this observed color change was structural or pigmentary in origin, we immersed individual scales in oil, which matches the refractive index of chitin and thereby suppresses structural coloration. As in previous studies, absorbance spectra collected under these refractive index-matched conditions provide a measure of the light transmitted through the scale and served as a proxy for pigment content, as differences in pigment type and concentration result in distinct patterns of wavelength-specific light absorption (Matsuoka and Monteiro 2018; Ren et al. 2020; Thayer et al. 2020; Prakash et al. 2022; Finet et al. 2023; Banerjee et al. 2024; Jessop et al. 2024) . We observed minimal differences in absorbance of visible wavelengths between mutant and wild-type scales (Fig. 1b; Table S2), indicating that the shift in coloration is primarily due to structural changes rather than differences in pigmentation.

To investigate the ultrastructural basis of the iridescent blue coloration in *araucan* mutant scales, we measured the thickness of the lower lamina—a key structural determinant of scale color in butterflies of the *Junonia* genus. A prior study has shown that thicker lower lamina causes a shift towards bluer hues (Thayer et al. 2020). We therefore quantified laminar thickness in both wild-type brown scales and blue mutant scales to assess whether this relationship held true in our *araucan* knockouts. SEM imaging after FIB milling to get the transverse section of scales revealed that mutant cover scales had significantly thicker lower laminae compared to wild type (Fig. 1c; LME model, AIC-selected best fit, $p < 2 \times 10^{-16}$; Tables 1, S1). The mean corrected lower lamina thickness in wild-type scales was 96.7 ± 10.2 nm, while mutant scales averaged 152.0 ± 18.9 nm, supporting the hypothesis that the observed color shift is structurally mediated.

To assess whether additional ultrastructural features contribute to the iridescent color shift observed in *araucan* mutants, after observing no apparent differences in the scale

ultrastructure, we quantified ridge spacing and crossrib distances in cover scales. These geometric features determine the size of the scale “windows” that determine the amount of incident light that interact with underlying scale nanostructures (Fig. 1d). Mean ridge-to-ridge spacing was comparable between wild-type brown and mutant blue scales (WT: 1921 ± 90 nm; mutant: 1921 ± 73 nm; Fig. 1d; Tables 1, S1), and crossrib distance was also unchanged (WT: 923 ± 167 nm; mutant: 914 ± 160 nm; Fig. 1d; Tables 1, S1). These results suggest that the shift to blue structural coloration in the *araucan* mutants is not due to changes in ridge or crossrib geometry, but instead is primarily driven by increased lower lamina thickness.

araucan knockouts eliminate purple-violet iridescence in forewing eyespot centers

Eight of the recovered *araucan* mKOs exhibited a striking phenotype affecting the scales in the forewing eyespot centers. In wild-type *J. coenia*, these eyespot centers exhibit a vivid purple-violet iridescence (Fig. 2a, S3). In contrast, *araucan* mutants lacked this strong purple-violet coloration, which was replaced by a muted grey-brown hue, occasionally with faint traces of pink or violet iridescence (Fig. 2a, S3). The loss of purple-violet iridescence was asymmetrical in all but two individuals (Fig. S3), validating the mosaic nature of the knockout phenotype. Notably, eyespot centres on the hindwings were unaffected.

The iridescent purple-violet coloration of *J. coenia* eyespot centres arises from the combined optical properties of both cover and underlying ground scales. The ground scales enhance the overall saturation of the reflected color when stacked beneath the more translucent cover scales (highlighted by yellow dashed outlines in Fig. 2a). Because this mechanism is consistent with observations in other butterfly species exhibiting purple-violet coloration (Giraldo et al. 2016; Siddique et al. 2016), we characterized the optical properties of each scale type within the eyespot center. Specifically, we measured reflectance spectra and refractive index-matched absorbance spectra of both cover and ground scales in the forewing eyespot center to identify which scale type and optical mechanism was contributing to the observed color shift.

Spectral analysis showed that both scale types, cover and ground, were altered in the *araucan* mutants differently, resulting in the observed color shift. Mutant cover scales exhibited increased reflectance above 500 nm, corresponding to a duller grey-brown coloration, whereas wild-type cover scales reflected more light in the ultraviolet to violet wavelengths (380–450 nm), producing the observed purple-violet hue (Fig. 2a, b). In contrast, reflectance measurements of ground scales revealed no significant differences between wild-type and mutant individuals (Fig. 2c). To assess pigment contributions independent of structural effects, we measured absorbance in a refractive index–matched medium. Under these conditions, both wild-type and mutant cover scales showed minimal light absorption in the ultraviolet and red regions, with no significant differences between groups, indicating that most incident light was transmitted through the cover scales (Fig. 2b). However, mutant ground scales showed a different pattern across the ultraviolet and visible spectrum (300–700 nm) where they exhibited significantly lower absorbance compared to wild-type scales, suggesting reduced pigmentation in the mutants (Fig. 2c).

To identify structural components in the scales that might have been altered, we characterized lamina thickness, ridge spacing, and crossrib distances in both cover and ground scales. We found that the lower lamina was significantly thicker in the eyespot scales of wild-type individuals compared to *araucan* mutants in both scale types. In cover scales, the lower lamina thickness averaged 151 ± 16.9 nm in wild types and 112 ± 13.1 nm in the mutants (LME model, AIC-selected best fit, $p < 2e\text{-}16$; Fig. 2d; Table 2, S3). A similar pattern was observed in ground scales (146 ± 13.9 nm in wild types vs 108 ± 10.3 nm in mutants, $p < 2e\text{-}16$; Fig. 2e; Table 2, S3).

Ridge spacing was significantly narrower in mutants versus wild-type scales, for both scale types. In cover scales, ridge spacing was 2123 ± 82.9 nm in wild types and 1805 ± 62.9 nm in mutants ($p < 2e\text{-}16$; Fig. 2d; Table 2, S3), and in ground scales, 1470 ± 116 nm in wild types versus 1188 ± 74 in mutants ($p < 2e\text{-}16$ Fig. 2e; Table 2, S3). In contrast, the distance between crossribs was significantly greater in *araucan* mutants

for both scale types. In cover scales, mutants had cross-rib spacing of 1202 ± 322 nm compared to 946 ± 217 in wild types (p < 2e-16 Fig. 2d; Table 2, S3); and in ground scales, mutants had 663 ± 103 nm of spacing vs 631 ± 79.3 nm in wild types (p = 1.42e-05; Fig. 2e; Tables 2e, S3). Together, these optical and structural analyses reveal that *araucan* knockouts disrupt the pigmentation of ground scales and the nanostructural organization of both cover and ground scales in the eyespot centers. These changes likely underlie the loss of saturated purple-violet iridescence and its replacement with muted hues in *araucan* mutants.

araucan is broadly expressed in nascent pupal scale cells

Our mKOs demonstrate that *araucan* is necessary for normal structural coloration of *J. coenia* wing scales and appears to play a role in determining scale structure itself. Accordingly, we hypothesized that we should observe *araucan* expression in wings during scale morphogenesis. We additionally wanted to ask if there might be any detectable pattern-specific expression associated with the mutant phenotypes we observed, for example in eyespot centers. To characterize spatial transcription patterns of *araucan*, we used HCR *in situ* hybridizations targeting *araucan* mRNA across key stages of wing development: (1) in the developing last instar wing discs, immediately after the transcription factor Spalt defines future eyespot domains (Reed et al. 2007; Oliver et al. 2012; Reed et al. 2020), and (2) in pupal wings at two time points - 13% pupal development, when eyespot centers have been established, and 25% pupal development when scale precursor begin to elongate to form mature scale cells (Dinwiddie et al. 2014).

Our experiments did not reveal expression of *araucan* in larval imaginal discs (Fig. S4a) or at 13 % pupal development (Fig. S4b). They did, however, reveal broad *araucan* expression across pupal forewings and hindwings at 25% pupal development (Fig. S4c). Clear staining occurred in staggered rows of cells corresponding to the alternating cover and ground scale cells (Fig. 3a). Three-dimensional confocal imaging revealed the highest levels of *araucan* transcripts localized to the apical extensions of nascent scales (Fig. 3b). While we did not observe spatial associations between *araucan* mRNA

abundance and adult color patterns during larval and early pupal wing development (Fig. S4), we cannot absolutely rule out color pattern associations at late stages of pupal development when scales are cuticularizing and *in situ* hybridizations are challenging. In any case, our *in situ* hybridizations are consistent with our knockout phenotypes in supporting a role for *araucan* specifically in wing scale development.

araucan is a direct target of the transcription factors Optix and Spalt

The phenotypes we observed in *araucan* knockouts are reminiscent of *optix* knockout phenotypes, which exhibit blue structural coloration in mutant clones in association with thickening of the lower lamina of scale cells (Fig. 1a, c) (Zhang et al. 2017; Thayer et al. 2020) . However, the phenotypes differed in that *araucan* mutants showed no obvious changes in dorsal color pigmentation, whereas *optix* knockouts exhibited a replacement of colored ommochromes by melanins, alongside their structural color phenotypes. Given that *araucan* phenotypes represent a subset of the broader *optix* knockout effects, we hypothesized that *optix* may affect structural coloration in part through regulation of *araucan*. Due to the developmental lethality and high mortality rate associated with *optix* G_0 knockouts, generating stable *optix* mutant lines to assess indirect regulatory effects is not currently feasible. To assess the possibility of a direct regulatory interaction, we performed ChIP-seq to examine binding of the Optix transcription factor at the *araucan* locus during pupal wing development (65 % pupal development). Indeed, we found that Optix binds to the *araucan* promoter, where it co-localizes with RNA polymerase II (Fig. 4, S5). Together, the knockout and ChIP-seq data suggests a model in which Optix is a direct positive regulator of *araucan* during wing development.

We were also intrigued by the effects of *araucan* on ground scale pigmentation especially evident in the eyespot centres and hypothesized that it might be regulated by an eyespot determining factor. To test this, we performed ChIP-seq for the transcription factor Spalt in fifth instar larval wings. Spalt is a key factor in the eyespot determination process – it is one of the earliest known genes to be expressed in the eyespots in larval imaginal discs, and its expression is maintained in eyespots into early pupal

development (Fig. S4) (Brunetti et al. 2001; Reed et al. 2007; Oliver et al. 2012; Stoehr et al. 2013; Reed et al. 2020). Spalt knockout phenotypes include complete loss of eyespots suggesting they are a master regulator of eyespot formation in these butterflies (Zhang and Reed 2016). Our ChIP-seq data reveal that Spalt binds to the *araucan* promoter, at the same location as Optix and RNA polymerase II (Fig. 4, S5). This apparent regulatory interaction between the eyespot determination factor Spalt and *araucan* provides a tentative mechanistic basis for the eyespot-specific phenotypes observed in *araucan* knockouts.

DISCUSSION

In this study, we investigated the role of the Iroquois-complex gene *araucan* in butterfly wing patterning. Our findings reveal that *araucan* is a key regulator of structural coloration in *J. coenia*, modulating iridescence in two spatially and functionally distinct ways: (1) by suppressing blue iridescence across the dorsal wing surface, and (2) by promoting purple-violet iridescence within forewing eyespot center.

Structural coloration in butterfly wings arises from complex interactions between incident light and the ultrastructure of wing scales, as reviewed by Thayer and Patel (Thayer and Patel 2023). One well-characterized mechanism is thin-film interference, in which the lower lamina of the scale functions as a reflective surface, producing a range of iridescent hues depending on its thickness and the angle of incident light (Stavenga et al. 2014; Wasik et al. 2014; Giraldo et al. 2016; Thayer and Patel 2023). Previous work in *Junonia spp*. has shown that the thickness of the lower lamina within individual cover scales reliably predicts spectral reflectance: thin laminae generate golden-brown hues as seen in wild type *J. coenia*, whereas thicker laminae produce blue or teal hues as seen in *optix* knockouts of *J. coenia* or species in the genus that naturally exhibit blue-green iridescence (Thayer et al. 2020). In our *araucan* knockouts, we observed an increase in lower lamina thickness in dorsal cover scales, resulting in a shift from brown to blue structural coloration. This optical shift occurred without detectable changes in scale pigmentation, or other scales indicating that *araucan* suppresses iridescence in non-eyespot regions by constraining laminar thickness.

In contrast, the eyespot centers of wild-type *J. coenia* display purple-violet iridescence that emerges from the combined optical effects of stacked cover and ground scales as shown in other nymphalid butterflies (Stavenga et al. 2014; Giraldo et al. 2016; Siddique et al. 2016). The ultrastructure and pigmentation of the cover scales modulates the amount of incident light reflected or transmitted, while those of the underlying ground scales influence the extent of light that is scattered back. Together, these layers generate interference patterns that either enhance or dampen the resulting color signal. In *araucan* mutants, we observed increased laminar thickness in both cover and ground scales, accompanied by a marked reduction in ground scale pigmentation. We infer that the loss of pigment decreases light absorbance, thereby increasing backscatter, which—when combined with structural modifications in the cover scales—produces a desaturated, muted tan-grey hue in place of the saturated purple-violet seen in wild-type eyespots. This enhanced backscatter likely contributes to the shimmering or hazy appearance of iridescence observed in some mutant individuals (Fig. S3). In addition, differences in ridge spacing and crossrib distances may further influence optical properties, either directly or by influencing pigmentation levels as seen before (Banerjee et al. 2024). Together, these findings demonstrate that *araucan* regulates multiple dimensions of scale morphology and composition that collectively shape the optical characteristics of forewing eyespot center coloration.

The opposing effects of *araucan* in eyespot versus non-eyespot scales underscore a broader principle in butterfly wing development: regulatory genes often function in a region-specific, context-dependent manner. The divergent roles of *araucan* reinforce the idea that eyespots represent modular, semi-independent developmental units capable of evolving specialized scale properties—including iridescence—without altering patterning in adjacent regions. This spatial modularity enables flexible evolutionary innovation within the wing, raising important questions about the regulatory architecture controlling *araucan* expression across the wing.

The transcription factors Optix and Spalt are known to be master regulatory switches of

blue structural coloration (Zhang et al. 2017) and eyespot determination respectively in *J. coenia* (Zhang and Reed 2016). Our whole wing, Spalt and Optix ChIP-seq results shows that they both bind to the *araucan* promoter during critical stages of wing development that include eyespot determination and scale structure development. These apparent regulatory interactions provide a clear and plausible model for how both Spalt and Optix can modulate iridescence in specific color pattern elements, such as eyespots, through a downstream *araucan*-mediated scale structure and scale pigmentation pathway. However, the lack of spatial or temporal co-expression data and functional validation limits our ability to draw definitive conclusions about their regulatory relationships. Testing the dynamic and region-specific interactions among *optix*, *spalt*, and *araucan* will be an important direction for future work.

In summary, our study identifies *araucan* as a necessary regulator of scale ultrastructure and structural coloration in butterflies. We reveal a regulatory mechanism that decouples eyespot and non-eyespot functions across the wing and provide genetic evidence that expands the known toolkit beyond *optix* for generating blue iridescent coloration. These findings offer new insight into the modular and evolvable architecture of butterfly wing patterning.

Data availability

The raw SEM images used for ultrastructural measurements, associated data tables, raw spectral data from scale micro-spectrophotometry, genome assembly and annotation files, and ChIP-seq signal tracks are available through Dryad (DOI: DOI: 10.5061/dryad.rfj6q57n6). All sequencing reads generated in this study have been deposited in NCBI under BioProject accession number PRJNA1268137.

Acknowledgements

This work features the undergraduate thesis research of Kate Siegel, and we would like to thank the Cornell MBG-GGD honors thesis program participants for support and feedback on the project. We thank Dr. Anyi Mazo-Vargas for use of her fluorescent microscope, Dr. Michael Perry for his gift of Spalt antibody, and Dr. Arnaud Martin for

his valuable feedback on the manuscript.

Funding

This work was supported by U.S. National Science Foundation GRFP DGE 2139899 to JMCM, by U.S. National Science Foundation grants IOS-2128164 and DEB-2242865 to RDR, SFARI 868055SEED Award to EM, Rand Wilbur V. Harlan Research Fellowship to LSL and the Ministry of Education (MOE) Singapore award MOE T2EP30222-0017 to CF and AM.

Conflict of Interest

The authors declare no conflict of interest.

REFERENCES

Banerjee TD, Finet C, Seah KS, Monteiro A. 2024. Optix regulates nanomorphology of butterfly scales primarily via its effects on pigmentation. Front Ecol Evol. 12. doi:10.3389/fevo.2024.1392050.

Brunetti CR, Selegue JE, Monteiro A, French V, Brakefield PM, Carroll SB. 2001. The generation and diversification of butterfly eyespot color patterns. Current Biology. 11(20):1578–1585. doi:10.1016/S0960-9822(01)00502-4.

Cavodeassi F, Modolell J, Gómez-Skarmeta JL. 2001. The Iroquois family of genes: from body building to neural patterning. Development. 128(15):2847–2855. doi:10.1242/dev.128.15.2847.

Chatterjee M, Yu XY, Brady NK, Hatto GC, Amendola CA, Reed RD. 2025. mirror determines the far posterior domain in butterfly wings. :2024.02.15.580576. doi:10.1101/2024.02.15.580576.

Dinwiddie A, Null R, Pizzano M, Chuong L, Leigh Krup A, Ee Tan H, Patel NH. 2014. Dynamics of F-actin prefigure the structure of butterfly wing scales. Developmental Biology. 392(2):404–418. doi:10.1016/j.ydbio.2014.06.005.

Fandino RA, Brady NK, Chatterjee M, McDonald JMC, Livraghi L, van der Burg KRL, Mazo-Vargas A, Markenscoff-Papadimitriou E, Reed RD. 2024. The ivory lncRNA regulates seasonal color patterns in buckeye butterflies. Proceedings of the National Academy of Sciences. 121(41):e2403426121. doi:10.1073/pnas.2403426121.

Ficarrotta V, Hanly JJ, Loh LS, Francescutti CM, Ren A, Tunström K, Wheat CW, Porter AH, Counterman BA, Martin A. 2022. A genetic switch for male UV iridescence in an incipient species pair of sulphur butterflies. Proc Natl Acad Sci U S A. 119(3):e2109255118. doi:10.1073/pnas.2109255118.

Finet C. 2024. Developmental genetics of cuticular micro- and nano-structures in insects. Current Opinion in Insect Science. 65:101254. doi:10.1016/j.cois.2024.101254.

Finet C, Ruan Q, Bei YY, You En Chan J, Saranathan V, Yang JKW, Monteiro A. 2023. Multi-scale dissection of wing transparency in the clearwing butterfly Phanus vitreus. Journal of The Royal Society Interface. 20(202):20230135. doi:10.1098/rsif.2023.0135.

Giraldo MA, Yoshioka S, Liu C, Stavenga DG. 2016. Coloration mechanisms and phylogeny of Morpho butterflies. Journal of Experimental Biology. 219(24):3936–3944. doi:10.1242/jeb.148726.

Gómez-Skarmeta J-L, Corral RD del, Calle-Mustienes E de la, Ferrés-Marcó D, Modolell J. 1996. araucan and caupolican, Two Members of the Novel Iroquois Complex, Encode Homeoproteins That Control Proneural and Vein-Forming Genes. Cell. 85(1):95–105. doi:10.1016/S0092-8674(00)81085-5.

Gómez-Skarmeta JL, Modolell J. 1996. araucan and caupolican provide a link between compartment subdivisions and patterning of sensory organs and veins in the Drosophila wing. Genes Dev. 10(22):2935–2945. doi:10.1101/gad.10.22.2935.

Hines HM, Papa R, Ruiz M, Papanicolaou A, Wang C, Nijhout HF, McMillan WO, Reed RD. 2012. Transcriptome analysis reveals novel patterning and pigmentation genes underlying Heliconius butterfly wing pattern variation. BMC Genomics. 13(1):288. doi:10.1186/1471-2164-13-288.

Ikmi A, Netter S, Coen D. 2008. Prepatterning the *Drosophila* notum: The three genes of the *iroquois* complex play intrinsically distinct roles. Developmental Biology. 317(2):634–648. doi:10.1016/j.ydbio.2007.12.034.

Jessop A-L, Pirih P, Wang L, Patel NH, Clode PL, Schröder-Turk GE, Wilts BD. 2024. Elucidating nanostructural organization and photonic properties of butterfly wing scales using hyperspectral microscopy. Journal of The Royal Society Interface. 21(218):20240185. doi:10.1098/rsif.2024.0185.

Kehl BT, Cho K-O, Choi K-W. 1998. mirror, a Drosophila homeobox gene in the iroquois complex, is required for sensory organ and alula formation. Development. 125(7):1217–1227. doi:10.1242/dev.125.7.1217.

Kerner P, Ikmi A, Coen D, Vervoort M. 2009. Evolutionary history of the iroquois/Irx genes in metazoans. BMC Evolutionary Biology. 9(1):74. doi:10.1186/1471-2148-9-74.

Langmead B, Salzberg SL. 2012. Fast gapped-read alignment with Bowtie 2. Nat Methods. 9(4):357–359. doi:10.1038/nmeth.1923.

Lewis JJ, van der Burg KRL, Mazo-Vargas A, Reed RD. 2016. ChIP-Seq-Annotated Heliconius erato Genome Highlights Patterns of cis-Regulatory Evolution in Lepidoptera. Cell Rep. 16(11):2855–2863. doi:10.1016/j.celrep.2016.08.042.

Lewis JJ, Geltman RC, Pollak PC, Rondem KE, Van Belleghem SM, Hubisz MJ, Munn PR, Zhang L, Benson C, Mazo-Vargas A, et al. 2019. Parallel evolution of ancient, pleiotropic enhancers underlies butterfly wing pattern mimicry. Proceedings of the National Academy of Sciences. 116(48):24174–24183. doi:10.1073/pnas.1907068116.

Lewis JJ, Reed RD. 2019. Genome-Wide Regulatory Adaptation Shapes Population-Level Genomic Landscapes in Heliconius. Molecular Biology and Evolution. 36(1):159–173. doi:10.1093/molbev/msy209.

Li Q, Brown JB, Huang H, Bickel PJ. 2011. Measuring reproducibility of high-throughput experiments. The Annals of Applied Statistics. 5(3):1752–1779. doi:10.1214/11-AOAS466.

Livraghi L, Hanly JJ, Loh LS, Henry A, Keck CMT, Shirey VM, Tsai C-C, Yu N, Belleghem SMV, Roberts WM, et al. 2025. Genetic basis of an adaptive polymorphism controlling butterfly silver iridescence. Current Biology. 0(0). doi:10.1016/j.cub.2025.03.028. [accessed 2025 Apr 12]. https://www.cell.com/current-biology/abstract/S0960-9822(25)00313-6.

Maia R, Gruson H, Endler JA, White TE. 2019. 2: New tools for the spectral and spatial analysis of colour in r. Methods in Ecology and Evolution. 10(7):1097–1107. doi:10.1111/2041-210X.13174.

Martin A, McCulloch KJ, Patel NH, Briscoe AD, Gilbert LE, Reed RD. 2014. Multiple recent co-options of Optix associated with novel traits in adaptive butterfly wing radiations. EvoDevo. 5:7. doi:10.1186/2041-9139-5-7.

Matsuoka Y, Monteiro A. 2018. Melanin Pathway Genes Regulate Color and Morphology of Butterfly Wing Scales. Cell Reports. 24(1):56–65. doi:10.1016/j.celrep.2018.05.092.

Oliver JC, Tong X-L, Gall LF, Piel WH, Monteiro A. 2012. A Single Origin for Nymphalid Butterfly Eyespots Followed by Widespread Loss of Associated Gene Expression. PLOS Genetics. 8(8):e1002893. doi:10.1371/journal.pgen.1002893.

Pinheiro J, Bates D, R Core Team. 1999. nlme: Linear and Nonlinear Mixed Effects Models. :3.1-168. doi:10.32614/CRAN.package.nlme. [accessed 2025 Apr 12]. https://CRAN.R-project.org/package=nlme.

Prakash A, Dion E, Banerjee TD, Monteiro A. 2024. The molecular basis of scale development highlighted by a single-cell atlas of Bicyclus anynana butterfly pupal forewings. Cell Reports. 43(5). doi:10.1016/j.celrep.2024.114147.

Prakash A, Finet C, Banerjee TD, Saranathan V, Monteiro A. 2022. Antennapedia and optix regulate metallic silver wing scale development and cell shape in Bicyclus anynana butterflies. Cell Reports. 40(1). doi:10.1016/j.celrep.2022.111052.

Ramírez F, Ryan DP, Grüning B, Bhardwaj V, Kilpert F, Richter AS, Heyne S, Dündar F, Manke T. 2016. deepTools2: a next generation web server for deep-sequencing data analysis. Nucleic Acids Research. 44(W1):W160–W165. doi:10.1093/nar/gkw257.

Reed RD, Chen P-H, Frederik Nijhout H. 2007. Cryptic variation in butterfly eyespot development: the importance of sample size in gene expression studies. Evolution & Development. 9(1):2–9. doi:10.1111/j.1525-142X.2006.00133.x.

Reed RD, Selegue JE, Zhang L, Brunetti CR. 2020. Transcription factors underlying wing margin color patterns and pupal cuticle markings in butterflies. EvoDevo. 11(1):10. doi:10.1186/s13227-020-00155-w.

Ren A, Day CR, Hanly JJ, Counterman BA, Morehouse NI, Martin A. 2020. Convergent Evolution of Broadband Reflectors Underlies Metallic Coloration in Butterflies. Front Ecol Evol. 8. doi:10.3389/fevo.2020.00206.

Robinson JT, Thorvaldsdóttir H, Winckler W, Guttman M, Lander ES, Getz G, Mesirov JP. 2011. Integrative Genomics Viewer. Nat Biotechnol. 29(1):24–26. doi:10.1038/nbt.1754.

Rodriguez-Caro F, Fenner J, Bhardwaj S, Cole J, Benson C, Colombara AM, Papa R, Brown MW, Martin A, Range RC, et al. 2021. Novel Doublesex Duplication Associated with Sexually

Dimorphic Development of Dogface Butterfly Wings. Molecular Biology and Evolution. 38(11):5021–5033. doi:10.1093/molbev/msab228.

Schindelin J, Arganda-Carreras I, Frise E, Kaynig V, Longair M, Pietzsch T, Preibisch S, Rueden C, Saalfeld S, Schmid B, et al. 2012. Fiji: an open-source platform for biological-image analysis. Nat Methods. 9(7):676–682. doi:10.1038/nmeth.2019.

Setton EVW, Ballesteros JA, Blaszczyk PO, Klementz BC, Sharma PP. 2024. A taxon-restricted duplicate of Iroquois3 is required for patterning the spider waist. PLOS Biology. 22(8):e3002771. doi:10.1371/journal.pbio.3002771.

Siddique RH, Vignolini S, Bartels C, Wacker I, Hölscher H. 2016. Colour formation on the wings of the butterfly Hypolimnas salmacis by scale stacking. Sci Rep. 6(1):36204. doi:10.1038/srep36204.

Stavenga DG, Leertouwer HL, Wilts BD. 2014. Coloration principles of nymphaline butterflies – thin films, melanin, ommochromes and wing scale stacking. Journal of Experimental Biology. 217(12):2171–2180. doi:10.1242/jeb.098673.

Stoehr AM, Walker JF, Monteiro A. 2013. Spalt expression and the development of melanic color patterns in pierid butterflies. EvoDevo. 4(1):6. doi:10.1186/2041-9139-4-6.

Thayer RC, Allen FI, Patel NH. 2020. Structural color in Junonia butterflies evolves by tuning scale lamina thickness. Tautz D, Desplan C, Jiggins C, editors. eLife. 9:e52187. doi:10.7554/eLife.52187.

Thayer RC, Patel NH. 2023. A meta-analysis of butterfly structural colors: their color range, distribution and biological production. Journal of Experimental Biology. 226(21):jeb245940. doi:10.1242/jeb.245940.

Villinger C, Gregorius H, Kranz C, Höhn K, Münzberg C, von Wichert G, Mizaikoff B, Wanner G, Walther P. 2012. FIB/SEM tomography with TEM-like resolution for 3D imaging of high-pressure frozen cells. Histochem Cell Biol. 138(4):549–556. doi:10.1007/s00418-012-1020-6.

Wasik BR, Liew SF, Lilien DA, Dinwiddie AJ, Noh H, Cao H, Monteiro A. 2014. Artificial selection for structural color on butterfly wings and comparison with natural evolution. Proceedings of the National Academy of Sciences. 111(33):12109–12114. doi:10.1073/pnas.1402770111.

Zhang L, Mazo-Vargas A, Reed RD. 2017. Single master regulatory gene coordinates the evolution and development of butterfly color and iridescence. Proc Natl Acad Sci U S A. 114(40):10707–10712. doi:10.1073/pnas.1709058114.

Zhang L, Reed RD. 2016. Genome editing in butterflies reveals that spalt promotes and Distal-less represses eyespot colour patterns. Nat Commun. 7:11769. doi:10.1038/ncomms11769.

Zhang L, Reed RD. 2017. A Practical Guide to CRISPR/Cas9 Genome Editing in Lepidoptera. In: Sekimura T, Nijhout HF, editors. Diversity and Evolution of Butterfly Wing Patterns: An

Integrative Approach. Singapore: Springer. p. 155–172. [accessed 2025 Apr 12]. https://doi.org/10.1007/978-981-10-4956-9_8.

Zhang Y, Liu T, Meyer CA, Eeckhoute J, Johnson DS, Bernstein BE, Nusbaum C, Myers RM, Brown M, Li W, et al. 2008. Model-based Analysis of ChIP-Seq (MACS). Genome Biology. 9(9):R137. doi:10.1186/gb-2008-9-9-r137.

Table 1. Comparison of wild-type and *araucan* mutant non-eyespot cover scale ultrastructural features.

Scale type	Factor	Comparison	Estimate	Std error	Z-value	Pr(>|z|)	95% CI
cover	Lower-lamina thickness	WT - mutant == 0	-55.41	2.93	-18.89	<2e-16 ***	[-61.16 ; -49.66]
cover	Distance ridge-ridge	WT - mutant == 0	0.54	0.54	10.13	0.05	[-19.32 ; 20.39]
cover	Distance crossrib-cross-rib	WT - mutant == 0	8.61	14.25	0.6	0.54	[-19.31 ; 36.54]

Table 2. Comparison of wild-type and *araucan* mutant cover and ground scale ultrastructural features collected from eyespot center.

Scale type	Factor	Comparison	Estimate	Std error	Z-value	Pr(>|z|)	95% CI
cover	Lower-lamina thickness	WT - mutant == 0	38.92	2.61	14.89	<2e-16 ***	[33.79 ; 44.04]
cover	Distance ridge-ridge	WT - mutant == 0	317.75	6.83	46.51	<2e-16 ***	[304.36 ; 331.14]
cover	Distance crossrib-cross-rib	WT - mutant == 0	-256.73	24.15	-10.63	<2e-16 ***	[-304.06 ; -209.40]
ground	Lower-lamina thickness	WT - mutant == 0	38.46	2.45	15.72	<2e-16 ***	[33.67 ; 43.25]
ground	Distance ridge-ridge	WT - mutant == 0	282.4	6.87	41.08	<2e-16 ***	[268.93 ; 295.88]
ground	Distance crossrib-cross-rib	WT - mutant == 0	-32.52	7.49	-4.34	1.42e-05 ***	[-47.20 ; -17.83]

FIGURE LEGENDS

Figure 1. *araucan* knockouts cause blue iridescence in dorsal hindwings by increasing lower lamina thickness of cover scales. (a) *araucan* mKO produces patches of blue iridescent scales in the dorsal hindwing. *Left*: Wild-type wing showing uniform golden-brown color. Adjacent are magnified views of individual cover scales from the same wing, with the abaxial surface (*top*) and adaxial surface (*bottom*) shown. Right: *araucan* mKO hindwing showing a mosaic patch of blue iridescent scales (*dashed line*). Adjacent are magnified views of mutant cover scales, revealing blue iridesence on both the abaxial (*top*) and adaxial (*bottom*) surfaces. Scale bar = 50 μm. Additional images of contralateral hindwings showing mutant blue iridescent scales are in Fig. S2. (b) Reflectance and absorbance spectra of cover scales confirm that the observed color shift is structural, not pigment-based. Solid lines indicate mean spectra; shaded regions represent standard deviation; asterisks mark wavelengths with significant differences between groups (**p-adj < 0.01; Table S2). (c) *Left:* SEM images of transverse sections from isolated cover scales, prepared by cryo-fracturing, show that wild-type scales (*top*) have a thinner lower lamina (LL; *grey shaded region*) compared to mutant scales (*bottom*). *Right*: Violin-box plot quantifies lower lamina thickness from FIB-milled isolated cover scales (***$p < 2 \times 10^{-16}$; Tables 1, S1). (d) Additional cover scale measurements: ridge-to-ridge spacing ($d_{R\text{-}R}$, *top left*), distance between crossribs ($d_{CR\text{-}CR}$, *top right*), and area of the windows (*teal*) - through which incident light goes into the scale (*bottom*, ns – not significant; Tables 1, S1).

Figure 2. *araucan* knockouts diminish purple-violet iridesence by altering cover scale reflectance, ground scale pigmentation, and the ultrastructure of both scale types in forewing eyespot centers. (a) On both dorsal (*left*) and ventral (*middle*) surfaces, forewing eyespot centers of wild-type individuals (*top*) exhibit distinct purple-violet iridescence, whereas *araucan* knockouts (*bottom*) show muted grey-brown scales (Fig. S3). Magnified images of the eyespot center (*right*) highlight the stacking arrangement of cover (c.s; *white border*) and ground scales (g.s; *yellow arrows where exposed and yellow dashed boundaries where overlaid by cover scales*). Overlaid ground scales

highlight saturation of overall color (*yellow dashed boundary*). Abwing surfaces of isolated cover and ground scales (*far right*) of wild-type (*top*) and mutant (*bottom*) scales. (b) Spectrophotometry of isolated cover scales and (c) ground scales from eyespot centers in wild-type and mutant forewings. Reflectance spectra (*left*) and absorbance spectra (*right*). Solid lines represent mean spectra; shaded areas indicate standard deviation; asterisks denote wavelengths with significant differences between groups (***p-adj < 0.001, **p-adj < 0.01; Table S4). (d–e) Violin-box plots quantifying ultrastructural features in cover scales (d) and ground scales (e) (***$p < 2 \times 10^{-16}$; Tables 2, S3).

Figure 3. *araucan* transcripts are localized to the apical extensions of scale cells early in pupal development. (a) A planar confocal section of the HCR *in situ* hybridization, at 25% pupal development, shows *araucan* transcripts localized to parallel rows of nascent scale cells. The staggering of the scale cells represents the alternating ground (*arrow heads*) and cover (*arrows*) scales. (b) A three-dimensional reconstruction of pupal wing shows a high density of epithelial nuclei, marked by DAPI, with *araucan* transcript *in situ* hybridization signal enriched in the apical growth region of scale cells, which extend out from the epithelial surface. Exemplar cells are outlined by white dashed lines to compare positions between panels.

Figure 4. Optix and Spalt bind to the *araucan* promoter during wing development. Integrated Genomics Viewer (IGV) screenshot showing ChIP-seq signal across a 100 kb window centered on the *araucan* locus. Tracks represent normalized bigWig signals for Spalt (pink) and RNA Polymerase II (Pol II; teal) from fifth instar larval imaginal discs, followed by Optix (*blue*) and Pol II (*teal*) from 65% pupal wing development. Signal tracks are shown as subtracted ChIP enrichment profiles (IP minus Input). Boxes below each track indicate significant peaks called using MACS3 (FDR q < 0.05), retained across at least two biological replicates (IDR p < 0.05). Optix and Spalt both show strong binding at the *araucan* promoter, overlapping with Pol II signal at the same locus and developmental stages, suggesting coordinated regulation of *araucan* transcription. Tracks of all the replicates are provided in Fig. S5.

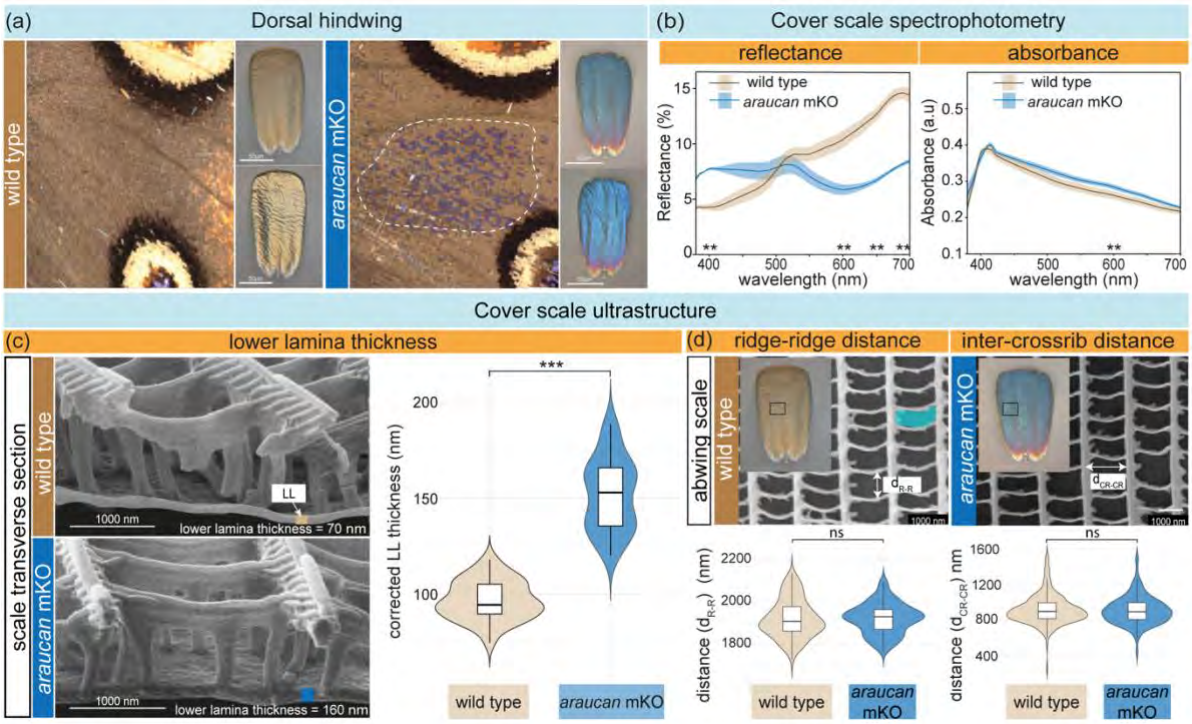
(a)
Dorsal hindwing
wild type
araucan mKO
(b)
Cover scale spectrophotometry
reflectance
absorbance
wild type
araucan mKO
Reflectance (%)
Absorbance (a.u)
wavelength (nm)
Cover scale ultrastructure
(c)
lower lamina thickness
scale transverse section
LL
1000 nm
lower lamina thickness = 70 nm
lower lamina thickness = 160 nm
corrected LL thickness (nm)
***
(d)
ridge-ridge distance
inter-crossrib distance
abwing scale
ns
distance (d R-R) (nm)
distance (d CR-CR) nm

Figure 1

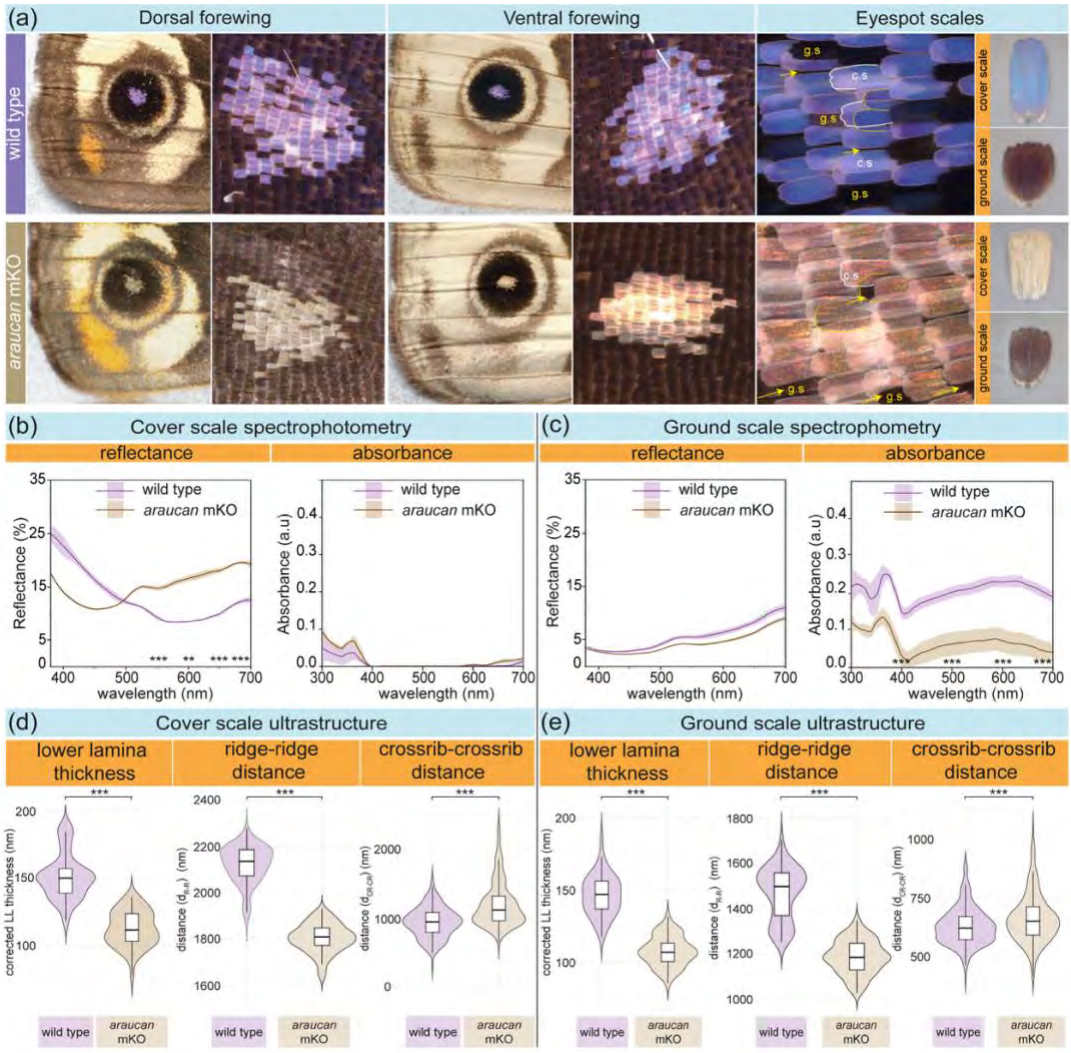
(a)
Dorsal forewing
Ventral forewing
Eyespot scales
wild type
araucan mKO
g.s
c.s
cover scale
ground scale
(b)
Cover scale spectrophotometry
reflectance
absorbance
wild type
araucan mKO
Reflectance (%)
Absorbance (a.u)
wavelength (nm)
(c)
Ground scale spectrophometry
(d)
Cover scale ultrastructure
lower lamina thickness
ridge-ridge distance
crossrib-crossrib distance
corrected LL thickness (nm)
(e)
Ground scale ultrastructure

Figure 2

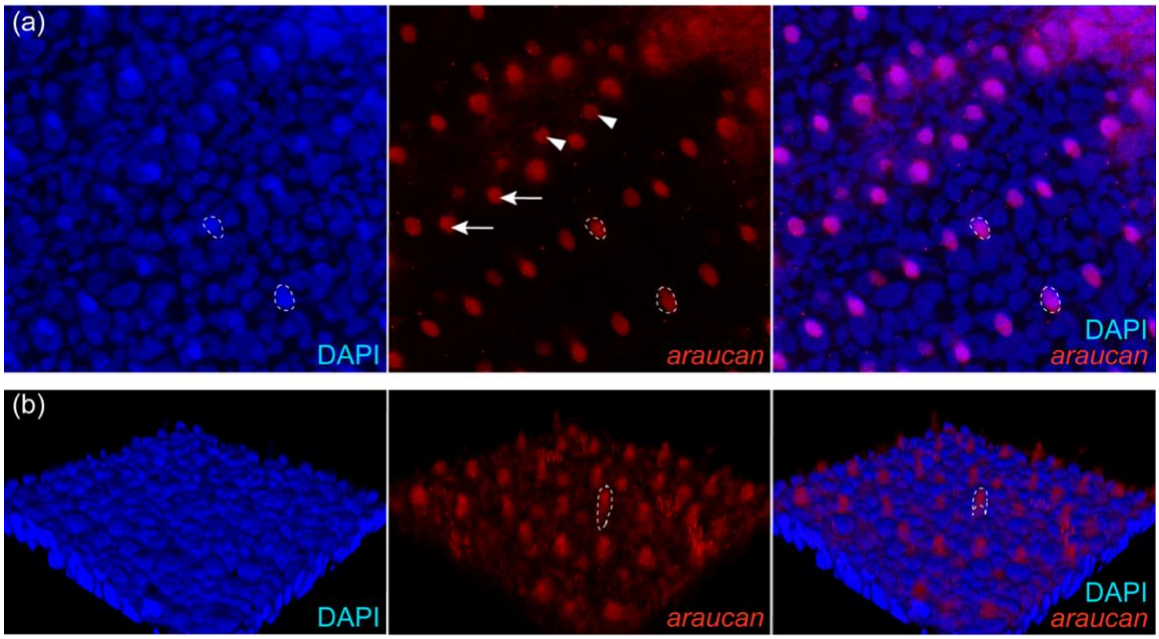

Figure 3

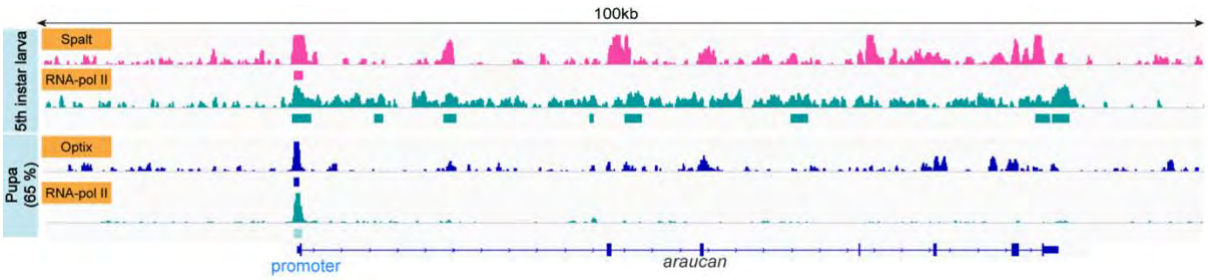
100kb
5th instar larva
Spalt
RNA-pol II
Pupa
(65 %)
Optix
RNA-pol II
promoter
araucan

Figure 4

SUPPLEMENTAL INFORMATION

FIGURES

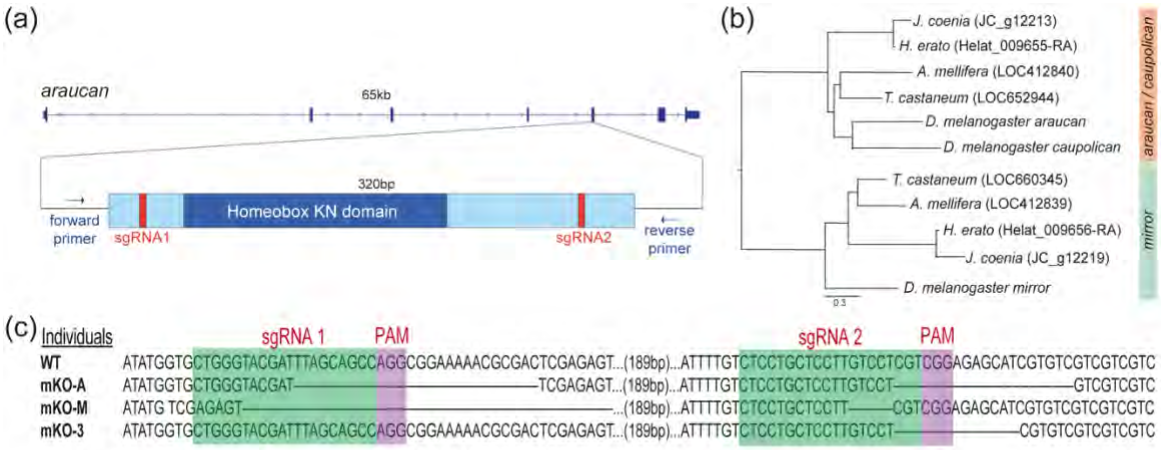

Figure S1. (a) Map of the *araucan* locus in *J. coenia,* annotated with the location of sgRNAs. The primers shown were used to validate deletions in mutants. Refer to Materials and Methods for the sequences of sgRNAs and genotyping primers. (b) Maximum likelihood phylogeny of *J. coenia*, *Heliconius erato lativitta*, *Tribolium castaneum*, *Apis mellifera*, and *D. melanogaster Iroquois* complex genes show that *JC_g12213* is the *araucan*/*caupolican* ortholog in *J. coenia* and JC_g12219 is the ortholog of *mirror*. Re-analysed already published data (Chatterjee et al. 2025), using new gene model identifiers. (c) CRISPR-Cas9 targeting of *araucan* produces deletions at the sgRNA sites. Wild type and mutant sequences are shown. Green boxes indicate sgRNA binding sites. Purple boxes denote PAM sites Knockouts mKO “A” and mKO “3” show blue dorsal iridescence phenotypes (Fig. S2). mKO M has eyespot focus phenotype (Fig. S2).

Figure S2. *araucan* mKOs displaying mutant patches (dashed lines) of iridescent blue scales (arrows). Contrasting lateral wings from individual butterflies are shown to highlight the asymmetrical nature of the mosaic phenotypes.

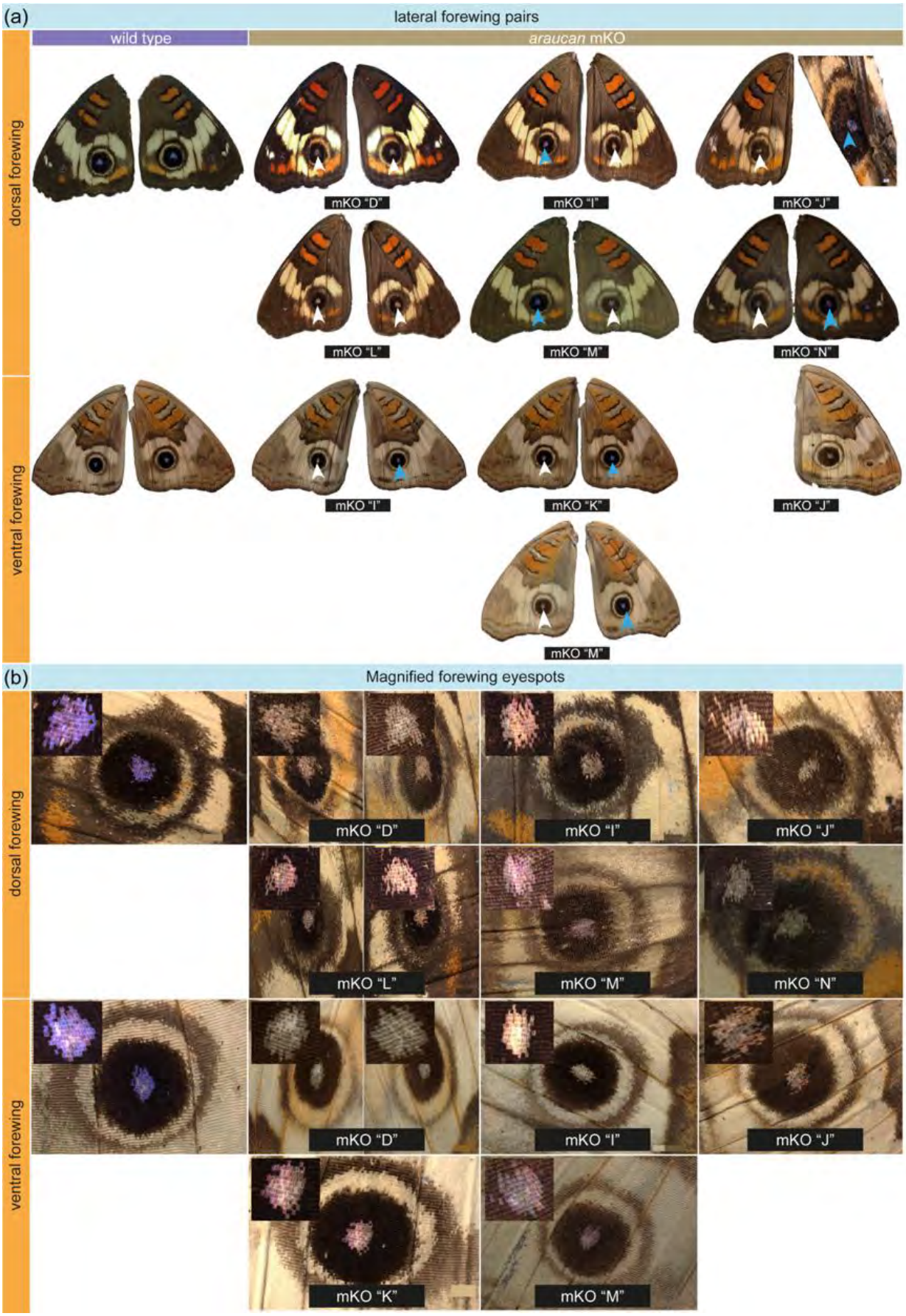
(a)
lateral forewing pairs
wild type
araucan mKO
dorsal forewing
ventral forewing
mKO "D"
mKO "I"
mKO "J"
mKO "L"
mKO "M"
mKO "N"
mKO "I"
mKO "K"
mKO "J"
mKO "M"
(b)
Magnified forewing eyespots
dorsal forewing
ventral forewing
mKO "D"
mKO "I"
mKO "J"
mKO "L"
mKO "M"
mKO "N"
mKO "D"
mKO "I"
mKO "J"
mKO "K"
mKO "M"

Figure S3. Loss of purple-violet iridescence in forewing eyespot foci following *araucan* mosaic knockout (mKO). (a) Contralateral forewings from representative individuals showing the elimination of purple-violet iridescence in dorsal (*top*) and ventral (*bottom*) eyespot foci. In most cases, both forewings exhibited the mutant phenotype, with exceptions noted in specimens "mKO D" and "mKO L." Blue arrows indicate wild-type foci with saturated iridescent coloration; white arrows indicate mutant foci displaying altered or absent iridescence. (b) Enlarged views of eyespot foci highlighting the phenotypic effects of *araucan* mKOs. Mutant scales show a range of altered hues, from muted grey to shimmering pink-purple, compared to the vivid purple-violet observed in wild type. Insets show scale-level differences in the dorsal (*top*) and ventral (*bottom*) surfaces.

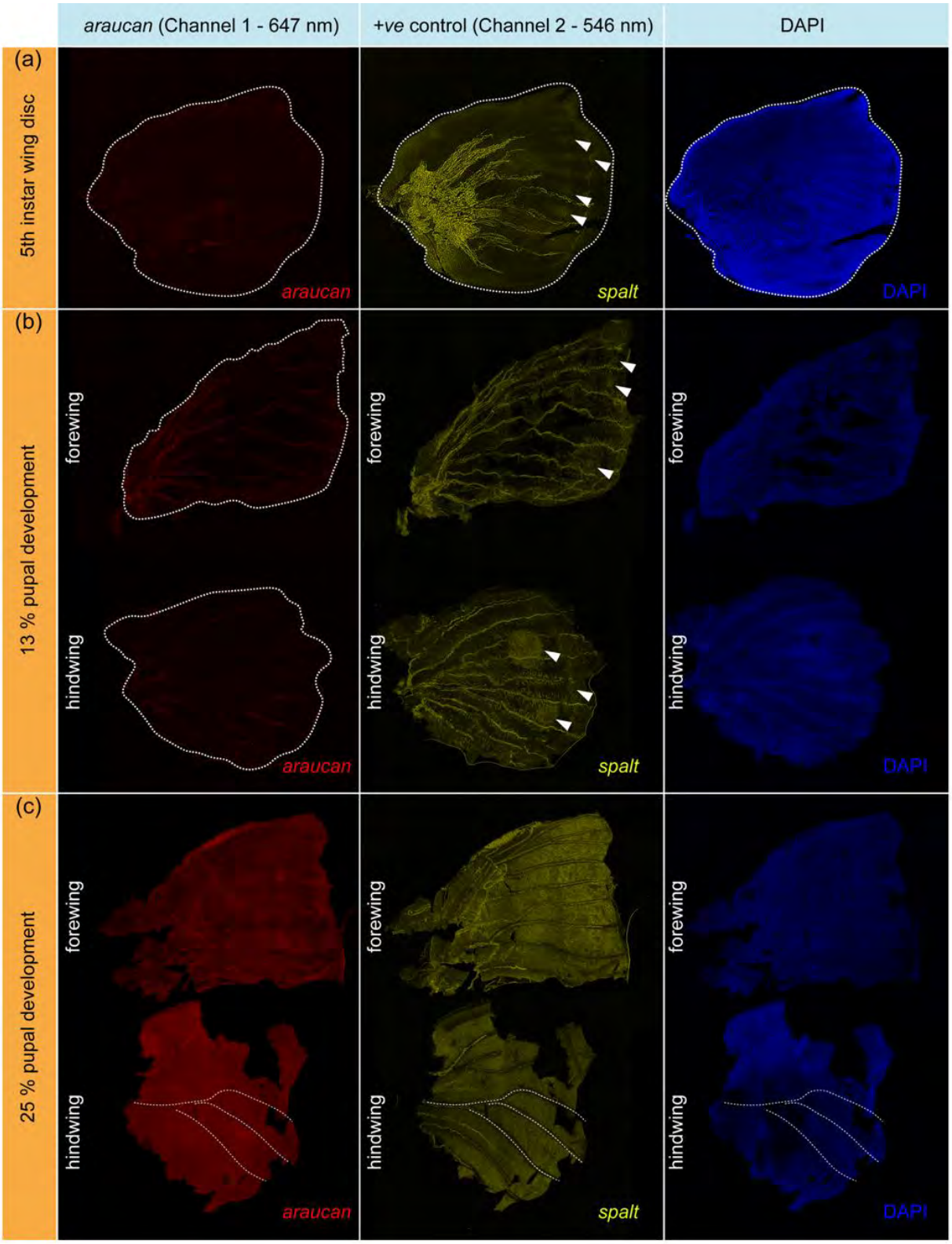

Figure S4. Expression of *araucan* across larval and pupal wing development. (a) Last instar wing discs: No detectable *araucan* expression (*left*), in contrast to *spalt* (yellow,

middle), which is expressed in a pattern-specific manner in the future eyespots and margin (*arrowheads*). DAPI (*right*) marks nuclei. (b) 13% pupal development: No detectable *araucan* expression in the forewing and hindwing (*left*), whereas *spalt* (yellow, *middle*) is broadly expressed, with higher expression in the eyespots and margin (*arrowheads*). DAPI (*right*) marks nuclei. (c) 25% pupal development: *araucan* (red, *left*) is expressed across the wing in a non-pattern-specific manner, like *spalt* (yellow, *middle*). DAPI (*right*) marks nuclei. White dotted lines denote wing boundaries and vein identifiers across corresponding images.

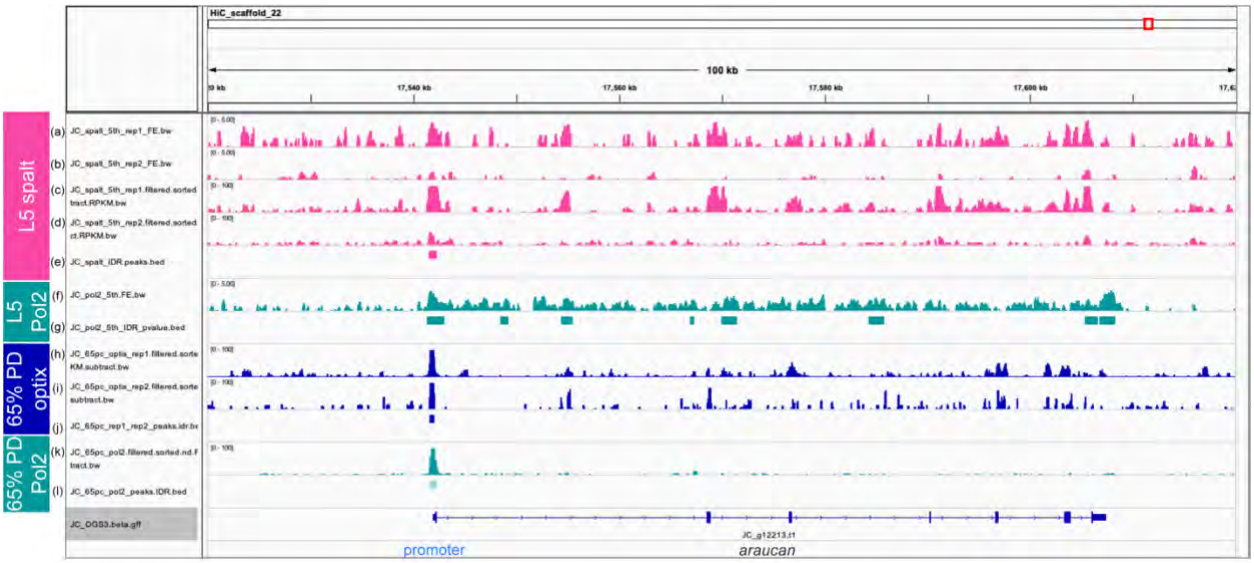

Figure S5. Spalt and Optix bind to the *araucan* promoter during late larval and mid-pupal development. Integrated Genomics Viewer (IGV) snapshots show ChIP-seq signal tracks for Spalt (pink), RNA Polymerase II (Pol II; teal), and Optix (blue) in a 100 kb region surrounding the *araucan* gene (*JC_g12213).* (a–b) Log_2 fold-enrichment bigWig tracks for two biological replicates of Spalt ChIP-seq over input control (range: 0–5), indicating enrichment at the *araucan* promoter. (c–d) Subtracted bigWig tracks (Spalt minus input) for the same replicates, showing read pileups (range: 0–100 reads) corresponding to specific binding regions. (e) Called peak (narrowPeak format) from Spalt ChIP-seq data consistent across replicates, confirming Spalt binding at the *araucan* promoter. (f–g) Pol II log_2 fold-enrichment signal and peak calls at late larval stage; the broad, non-sharp peak shape is consistent with active transcription. (h–j) Optix ChIP-seq replicates and peak call at 65% pupal development, indicating stage-specific binding at the *araucan* promoter consistent across two replicates. (k–l) Pol II ChIP-seq at 65% pupal development, showing a sharp, localized enrichment at the promoter, characteristic of transcriptional pausing.

TABLES

Table S1. Comparison of wild-type and *araucan* mutant non-eyespot cover scale ultrastructural features.

scale type	factor	numDF	denDF	F-value	P-value
cover	lower lamina thickness	1	94	356.72	<.0001
cover	distance ridge-ridge	1	244	0.003	0.96
cover	distance crossrib-crossrib	1	494	0.37	0.55

Table S2. Significance table of reflectance and absorbance spectra measured at different wavelengths.

Spectral type	Region -scale type	Wavelengths(nm)	p_value	p_adjusted	Significance
Absorbance	Non-eyespot-cover	350	0.0422	0.0562	ns
Absorbance	Non-eyespot-cover	400	0.5401	0.5401	ns
Absorbance	Non-eyespot-cover	450	0.0897	0.1026	ns
Absorbance	Non-eyespot-cover	500	0.02717234	0.043475744	*
Absorbance	Non-eyespot-cover	550	0.013793224	0.027586449	*
Absorbance	Non-eyespot-cover	600	0.001034415	0.008275317	**
Absorbance	Non-eyespot-cover	650	0.003316206	0.012877401	*
Absorbance	Non-eyespot-cover	700	0.004829025	0.012877401	*
Reflectance	Non-eyespot-cover	350	0.058198	0.066512	ns
Reflectance	Non-eyespot-cover	400	0.000189	0.001511	**
Reflectance	Non-eyespot-cover	450	0.012675	0.020281	*
Reflectance	Non-eyespot-cover	500	0.798358	0.798358	ns

Reflectance	Non-eyespot-cover	550	0.032901	0.043868	*
Reflectance	Non-eyespot-cover	600	0.002676	0.005351	**
Reflectance	Non-eyespot-cover	650	0.002317	0.005351	**
Reflectance	Non-eyespot-cover	700	0.002275	0.005351	**

Table S3. Comparison of wild-type and *araucan* mutant cover and ground scale ultrastructural features collected from eyespot center.

scale type	factor	numDF	denDF	F-value	P-value
cover	lower lamina thickness	1	94	221.66	<.0001
cover	distance ridge-ridge	1	244	2163.07	<.0001
cover	distance crossrib-crossrib	1	494	113.02	<.0001
ground	lower lamina thickness	1	98	247.29	<.0001
ground	distance ridge-ridge	1	244	1687.48	<.0001
ground	distance crossrib-crossrib	1	494	18.84	<.0001

Table S4. Significance table of reflectance and absorbance spectra measured at different wavelengths.

Spectral type	Region - scale type	Wavelengths(nm)	p_value	p_adjusted	Significance
Reflectance	Eyespot-ground	350	0.425298076	0.4252981	ns
Reflectance	Eyespot-ground	400	0.153736635	0.175699	ns
Reflectance	Eyespot-ground	450	0.080597206	0.1289555	ns
Reflectance	Eyespot-ground	500	0.035926762	0.0958047	ns
Reflectance	Eyespot-ground	550	0.098515912	0.1313545	ns
Reflectance	Eyespot-ground	600	0.024533269	0.0958047	ns
Reflectance	Eyespot-ground	650	0.002884728	0.0230778	*
Reflectance	Eyespot-ground	700	0.05407291	0.1081458	ns
Reflectance	Eyespot-cover	350	0.227171385	0.2596244	ns
Reflectance	Eyespot-cover	400	0.015502189	0.0206696	*
Reflectance	Eyespot-cover	450	0.00821814	0.013149	*
Reflectance	Eyespot-cover	500	0.676972861	0.6769729	ns
Reflectance	Eyespot-cover	550	0.000250499	0.0006858	***

Reflectance	Eyespot-cover	600	0.002863243	0.0057265	**
Reflectance	Eyespot-cover	650	0.000257188	0.0006858	***
Reflectance	Eyespot-cover	700	8.9404E-05	0.0006858	***
Absorbance	Eyespot-ground	350	0.308651917	0.3086519	ns
Absorbance	Eyespot-ground	400	8.29698E-05	0.0001673	***
Absorbance	Eyespot-ground	450	0.000106884	0.000171	***
Absorbance	Eyespot-ground	500	0.000158422	0.0001811	***
Absorbance	Eyespot-ground	550	8.3648E-05	0.0001673	***
Absorbance	Eyespot-ground	600	5.60723E-05	0.0001673	***
Absorbance	Eyespot-ground	650	0.000147918	0.0001811	***
Absorbance	Eyespot-ground	700	1.30136E-05	0.0001041	***

FILES

File S1. mRNA and amino acid sequences of genes used in this study, along with their *D. melanogaster* orthologs. These sequences were used to construct the gene family phylogeny shown in Figure S1b and to design probes for HCR *insitu* hybridization.

File S2. Sequences of *araucan* and *spalt* HCR-probes used for *in situ* hybridization.